IMPACT RESISTANT SUPERSTRUCTURE FOR POWER PLANTS PART I: BOX GIRDERS AND CONCRETE QUALITIES

W. Riedel[1], A. Stolz[1], Ch. Roller[1], M. Nöldgen[2], A. Laubach[2], G. Pattberg[3]
[1] Fraunhofer Institute for High-Speed Dynamics, Ernst-Mach-Institut, D-79588 Efringen-Kirchen, Germany
[2] Schüßler-Plan Ingenieurgesellschaft mbH, 40470 Düsseldorf, Germany
[3] AREVA NP GmbH, 63067 Offenbach, Germany
E-mail of corresponding author: werner.riedel@emi.fraunhofer.de

ABSTRACT

This paper describes the basic analysis of local resistance behavior against aircraft impact for a new structural concept to protect existing power plants. Two-Degree-of-Freedom (TDOF) models for the local shear and bending resistance are used and validated together with FEM for conventional concrete and UHPC. Conventional, standardized high strength and ultra-high strength concrete walls and T-sections of the protecting box girder structure are compared. The influence of tensile preloading in the wide spanning, bridge-type construction is quantified in finite element calculations with state of the art dynamic material descriptions. Necessary wall thicknesses to assure impact resistance by the high-performance box girders are key input to the structural design in part II.

INTRODUCTION

In the early 1970s many commercial nuclear power plants were designed against severe loading and accident scenarios such as earthquake, fire and flooding, but not to withstand aircraft crashes. In Germany "RSK" guidelines for reinforcing of succeeding plant generations against this accident type evolved in the following two decades [1][2][3] and were underlined by the crash of a Mirage fighter aircraft in March 1988 near Ohu. Since September 2001 intentional aircraft impact of civilian airliners is furthermore in discussion for safety requirements.

Strengthening of early plant generations requires additional protection structures to cope with the huge dynamic forces and momentum. In the present work a new concept for a superstructure to protect a boiling water reactor without direct contact to the existing buildings has been developed. The bridge-type, hollow box girder structure is illustrated in Fig. 1. The overall concept and its global structural load carrying properties are described in part II of the twin papers. One key aspect is the fact that the existing plant and its operation license are virtually unaffected by the construction.

However, while 1.8m wall thickness of conventional concrete are typical for existing aircraft-proof reactor buildings constructions, such dimensions and weights seem not applicable for the described free-spanning concept. Therefore, box girder design principles with higher and ultra-high strength concrete qualities are considered in chapter 3. The methods to assess the local penetration and perforation resistance are introduced in chapter 2. Two-Degree-of-Freedom (TDOF) and explicit Finite-Element-Methods (FEM) are shortly summarized and validated.

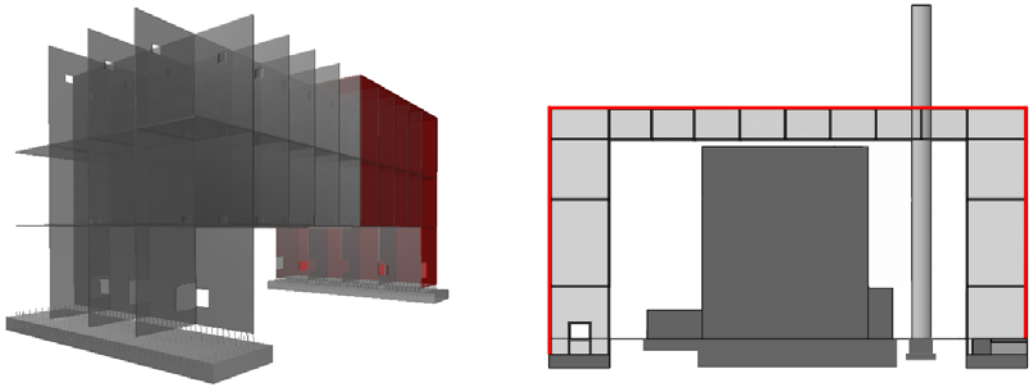

Fig. 1: Free-spanning superstructure concept protecting a boiling water reactor type against civilian and military aircraft; left: partly opened 3D view of the security hull (red) onto the bracing structures

METHODS AND VALIDATION FOR LOCAL IMPACT RESISTANCE

The following chapter presents different methods to predict the damage to a power plant caused by an aircraft impact. The quality is verified against well characterized "Meppen" tests with conventional strength concrete, especially tests II/4 and II/6 [4]. In these experiments, a steel tube with an effective mass of 1 ton impacted reinforced concrete slabs with velocities between 200 and 250 m/s. The transient load-time function can be derived as described Riera [5] and is used to evaluate the proposed analysis methods (see also [6]).

$$\begin{aligned} &\text{Meppen II/4} \quad V_{Ed} = 13.12\ \text{MN} < V_{Rd,sy} = 13{,}7\ \text{MN} \\ &\text{Meppen II/6} \quad V_{Ed} = 13.74\ \text{MN} < V_{Rd,sy} = 12{,}6\ \text{MN} \end{aligned} \tag{1}$$

DIN 25449 [7] describes the evaluation of a modified, empirical punching strength. The design code differentiates for V_{Rd} between components with and without stirrup reinforcement. The virtual loading V_{Ed} and the calculated $V_{Rd,sy}$ are compared. In order to take the dynamics into account static substitute loads and dynamic strength increase factors are calculated. Without these contributions equation 1 shows the comparison of the Meppen experiments and the design code calculations. An acceptable agreement is stated, but only if the static substitute factor and dynamic increase factor can be set to 1. In the following more enhanced calculation models will be discussed taking dynamics fully into account.

Two-Degree-of-Freedom Engineering Model

The TDOF model represents a simplified engineering model of the dynamic equilibrium during an impact, well suited for fast designs of components under combined shear and bending stresses. The basic equations used in the following were derived by Schlüter [6] and applied and modified by the authors. Both local effects of shearing or punching and global bending behavior are modelled according to Fig. 2 by a coupled system of two masses and two springs. M_1 and R_1, represent the global bending effects of the system, M_2 and R_2 describe the local effects of the conical shaped shear plug being pushed out of the slab. Whether the system undergoes both effects simultaneously or just one of them depends on the loading and the properties of the concrete component. The damping of the system (c_1, c_2 and c_3) takes into account the energy dissipation capacity of the oscillating slab and the punching process, primarily through internal friction and yielding. The corresponding time-dependent displacements w_1 (bending) and w_2 (shear) in the resulting coupled differential equations (2) are calculated in a fourth order Runge-Kutta time stepping scheme. The relative displacement u of the two masses quantifies punching motion.

$$\begin{aligned} M_1\ddot{w}_1 + c_1\dot{w}_1 + R_1(w_1) - R_2(u) - c_2\dot{u} &= 0 \\ M_2\ddot{w}_2 + c_2\dot{u} + c_3\dot{w}_2 + R_2(u) - F(t) &= 0 \end{aligned} \tag{2}$$

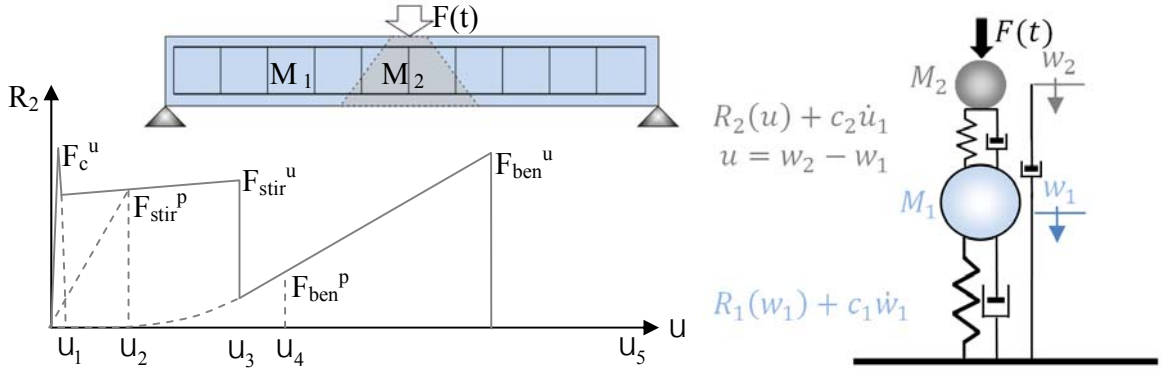

Fig. 2: TDOF model of local shear (M2) and bending resistance (M1), with the shape of the punching resistance function for reinforced concrete with shear and bending reinforcement

The effective bending mass M_1 can be derived by comparing the kinetic energy of the structure with the substituted mechanical system. The shear mass M_2 is defined by the geometrical dimensions of the punching cone. The resistance function R_1 describes the global elastic-plastic system behaviour of the reinforced concrete

undergoing structural bending, using the plastic moment capacity and the associated deformation. The resistance function for the shear loading R_2 material consists of a three phase failure model shown in Fig. 2. The deformation phases can be divided in a concrete failure, characterized by the maximum concrete tension force F_c^u, followed by the yielding of the stirrup reinforcement F_{stir}^p and rupturing F_{stir}^u. The last phase describes yielding und rupturing of the bending reinforcement. A detailed derivation of the applied TDOF model parameters is given in [8].

The diagrams in Fig. 3 compare the measurements of the Meppen tests II/4 and II/6 with the calculations of the TDOF model. The bending behaviour of the reinforced concrete slabs is calculated in both cases very well with the engineering model. In test II/4 the shear deformation is slightly underestimated by the model. For test II/6 the global structural bending behaviour and the local shear measurements are reproduced a very well. In summary, good predictive capabilities of the fast-running analysis tool can be stated. The transparent dynamic coupling of dynamic loading and structural deformation mechanisms is helpful to the designer.

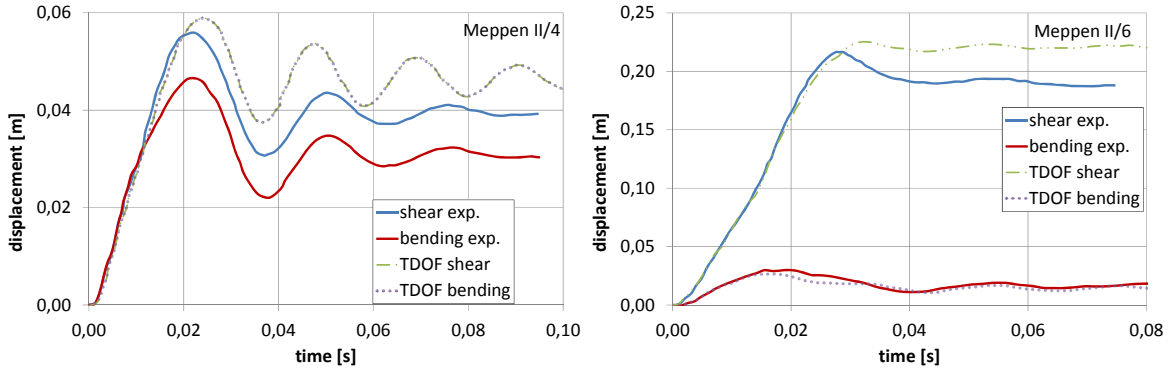

Fig. 3: Comparison of TDOF predictions (dashed) to two Meppen impact experiments (solid). Left, test II/4: shearing underestimated, bending very well predicted; right, test II/6: shearing and bending very well predicted

Finite-Element-Method

Wave propagation codes or 'hydrocodes' have become a powerful tool for analysing the impact induced stress waves and the resulting deformation and damage in various materials [9]-[12]. This special class of Finite-Element-Methods solves differential equations derived from the conservation laws for mass, momentum and energy together with the equations of state and the constitutive strength of the material. Explicit time integration schemes with small time steps resolve the highest frequency contents of stress wave propagation in the considered medium and the arising geometrical und material conditioned non-linearity during the dynamic deformation. The following numerical simulations in 2 and 3 dimensions were accomplished using the commercial hydrocode ANSYS AUTODYN [13].

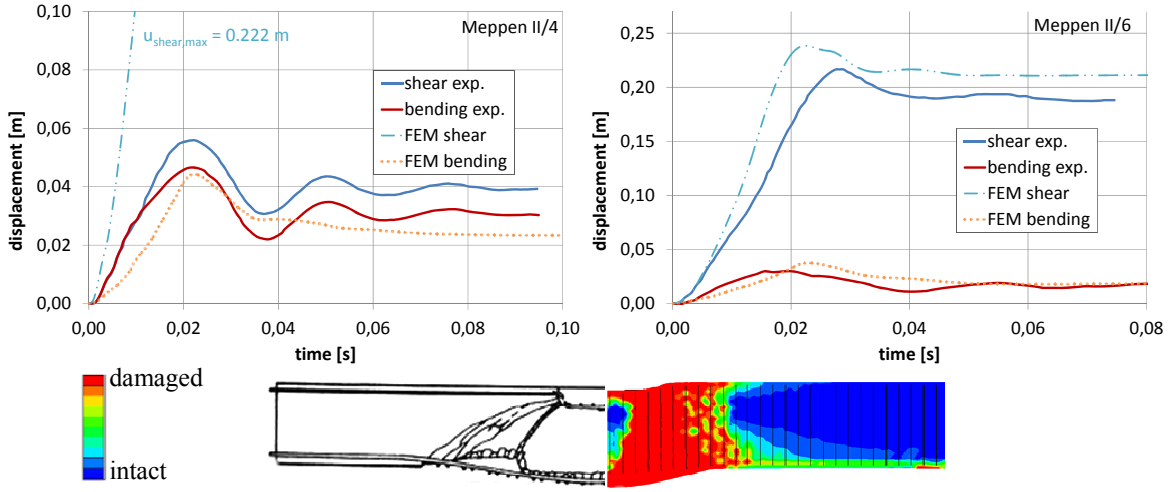

Fig. 4: Validation of explicit FE-Method with discrete rebar and RHT-concrete model for Meppen test II/4 and II/6

All reinforcements are discretized with discrete steel rebar elements described by the well-known Johnson-Cook material model [14] for strain and strain-rate hardening and thermal softening with strain based failure criteria. Concrete is described with the RHT-material model [11],[15]. The strength is modelled by three surfaces representing elastic limit, failure surface and residual strength including a continuum damage approach.

The quality of the cylindrical symmetric numerical simulations is again assessed against Meppen tests II/4 and II/6. Fig. 4 shows the calculated displacements curves for bending and shear deformations of the reinforced concrete slab. For II/4 the finite element system calculates a too weak shear resistance of the slab with a plug deformation by about 200 mm. Bending is well matched with slight under-prediction. The simulation of II/6 shows for shear and bending behaviour good agreement. Furthermore the outer shape and dimensions of the punching cone in the slab are calculated in good correlation to the experimental observations in Fig. 4, lower. The red coloured regions represent highly damaged concrete with multiple macroscopic crack patterns.

Table 1: DIN, TDOF and FEM models compared to Meppen experiments [4] on conventional concrete

analysis method	DIN 25449		TDOF		FEM	
resistance evaluation / experiment	shear	bending	shear	bending	shear	bending
Meppen II/4	~ correct*	n.c.	too high	correct	too low	correct
Meppen II/6	~ correct	n.c.	correct	correct	correct	correct

n.c.: not considered; * slightly too high

Table 1 summarizes the different analysis methods regarding their prediction quality compared to the Meppen experiments. Application of DIN 25449 delivers results with an acceptable bond on the shear loading, yet does not consider bending and dynamic coupling. TDOF and FEM show in some details slight differences but provide together a consistent picture with good predictive capabilities. For this reason their combination is used for the further analysis on different concrete qualities and complex 3D situations in the impact resistant superstructure.

Validation for Ultra-High Performance Concrete

For the new design construction elements with high and ultra-high performance are considered. The potential of fiber reinforced ultra-high performance concrete (UHPC) was analyzed in an engine impact test

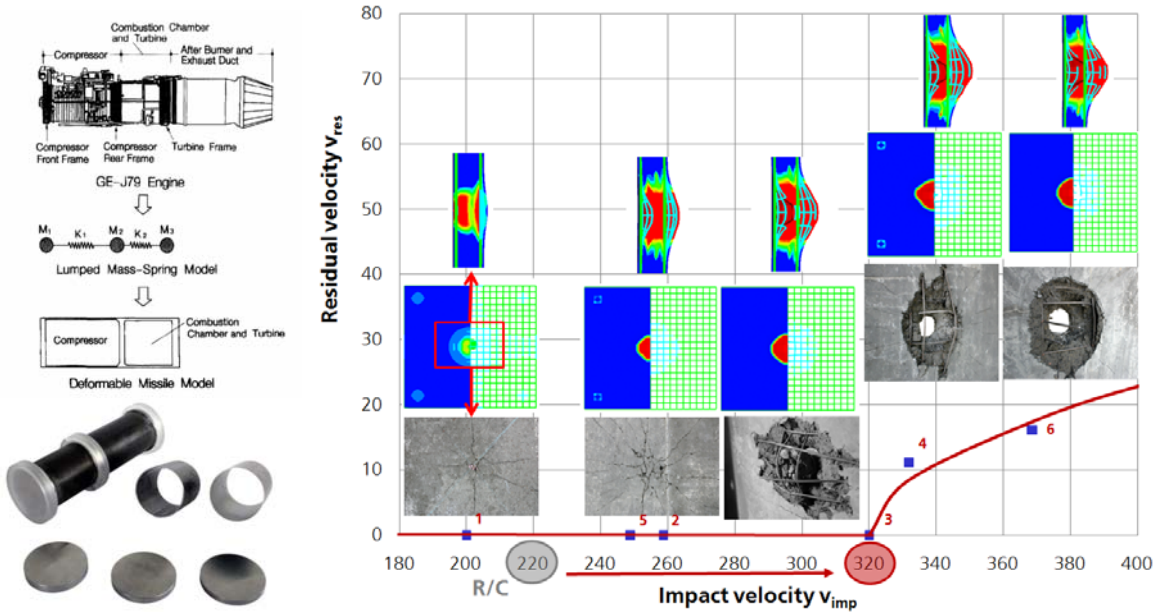

Fig. 5: Engine impact model approach by Sugano et al. [16]; increased ballistic limit from 219 m/s for conventional concrete to 320 m/s ± 10 m/s in recent tests with UHPC panels and validation of FE calculations in [8],[18]

campaign by the authors [12],[18]. In this work the original experimental strategy of Sandia National Laboratories [16] was extended to the fiber reinforced UHPC quality "B4Q" developed by the University of Kassel [17].

Fig. 5 shows the engine model components and the experimental configuration with an air gun of caliber 90 mm. The results are displayed in terms of residual over impact velocity and associated damage modes of the slabs. The ballistic limit of the UHPC B4Q with 1 % of steel fibers increased to 320 m/s compared to 219 m/s for identical conventional concrete plates. Hence the maximum momentum capacity is increased by to 50 %, the absorbed kinetic energy by remarkable 110 %.

The numerical simulations of the experiments with TDOF on the one hand and Finite-Element models using a modified RHT-model for the B4Q in combination with explicit rebar on the other hand showed good agreement in terms of the different observed failure modes and bearing capacity of the UHPC [8]. HPC strength data was not characterized and validated in detail, but interpolated between the well-based strength and equation of state data of UHPC and conventional concrete, with a reasonable degree of confidence.

LOCAL IMPACT RESISTANCE FOR HIGH PERFORMANCE BOX GIRDERS

A key task in designing an impact resistant superstructure is to avoid any perforation of the outer hull, before global load bearing comes into play. With the above methods, numerous investigations with different concrete qualities and varying levels of pre-loading were conducted to design a single-leaf protection layer for the hollow box girder structure shown in Fig. 1 and described in paper II. Selected results are presented in the following.

Comparison of Concrete Qualities using FEM

Starting from UHPC, the application of HPC with compressive cylinder strength of 80 and 100 MPa was considered for the determination of minimum wall thickness of the superstructure, since the economic advantage and applicability of HPC are attractive. The load cases of military aircraft (RSK) and civilian airliner where considered. The simulations where performed in 3D, using 5 volume elements for the concrete across the thickness, explicit rebar beams and material data as described in section 2 and the appendix.

Table 2 displays the result: For the military aircraft impact case a wall thickness of 90 cm is sufficient for all 3 concrete qualities. Concerning the civilian aircraft this dimension is only sufficient in the case of UHPC. The high performance concrete types display similar resistance behaviour if a component thickness of 100 cm is chosen.

Table 2: Limit thicknesses for high strength and ultra high strength concrete targets (reinforcement degree 120 m²/m) for impact by one chosen military and one civilian airliner; no pre-loading considered

wall thickness	UHPC		HPC 100		HPC 80	
[cm]	military	civilian	military	civilian	military	civilian
70	X	X	X	X	X	X
80	(X)	X	(X)	X	(X)	X
90	√	√	√	X	√	X
100	(√)	(√)	(√)	√	(√)	√
110	(√)	√	(√)	√	(√)	√
√ = sufficient resistance; X = no sufficient resistance; () = no consideration						

Limit Thickness with Static Pre-load predicted by FEM and TDOF

The structural calculations of the entire superstructure show areas of substantial tensile stresses from dead weight and variable actions resulting in non-negligible pre-load of the concrete and reinforcement. To capture this in the dynamic calculations, reduced yield and tensile strength of the rebar and concrete were considered matching the remaining strength to the load reserve in the pre-loaded structure. In addition to 3-D finite element simulation, a TDOF model was used for dimensioning the protective wall. For the same material, cross-section and impact load, beginning shear localization develops for preload considered (Fig. 6, right), both in FEM and TDOF simulations.

The evaluation is given in Table 3 for the HPC with compressive cylinder strength of 80 MPa and the decisive load case of a civilian aircraft. A wall design of 110 cm high performance concrete with corresponding flexural reinforcement and stirrups is recommended.

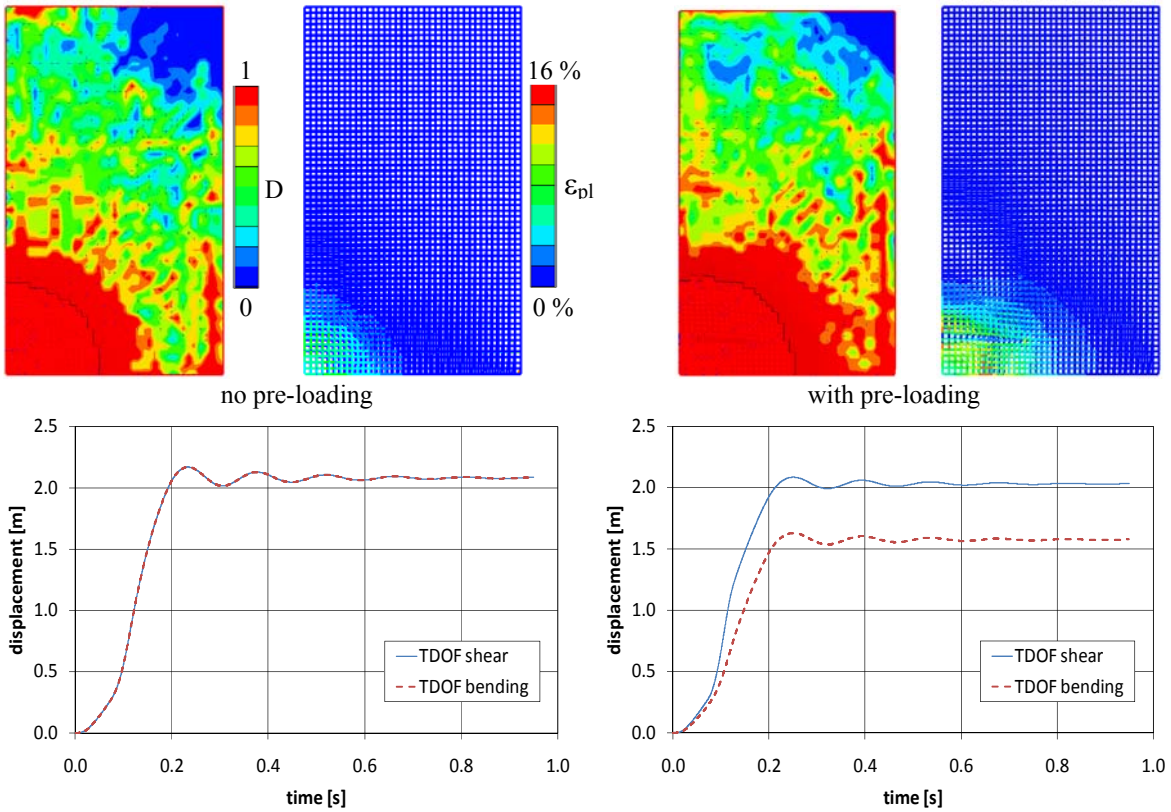

Fig. 6: Comparison of concrete damage D (HPC 80) and local plastic strain ε_{pl} in rebar without (left)) and with (right) preload; 40 % preload of rebar yield stress and 30 % tensile pre-damage assumed; damage extension is larger and localisation of the rebar starting in the case of pre-load (right)

Table 3: TDOF and FEM predictions of single layer HPC limit thickness against perforation by the assumed civilian airliner with and without pre-load; 110 cm limit thickness are deduced for the hull of the superstructure

wall thickness [cm]	concrete pre-damage [%]	reinforcement pre-load [%]	TDOF	3D-FEM	conclusion
100	0	0	√	√	√
100	0	20	√	√	√
100	0	40	√	X	X
100	30	40	√	X	X
110	0	40	(√)	√	√
110	30	20	(√)	√	√
110	30	40	√	√	√
√ = sufficient resistance; X = perforation; () = no consideration					

Consideration of T-Sections and Supports

Further load cases regarding impact in corner and edge regions were investigated. Here load transfer and damage propagation in bracing walls are relevant additionally to the punching resistance. The modeled section includes the outer high performance concrete bulkhead wall and floor level together with the conventional concrete walls and slabs behind (t_i = 50 cm) which form a bracing cross. The impact load acts centrically on the bracing cross straight onto the front face.

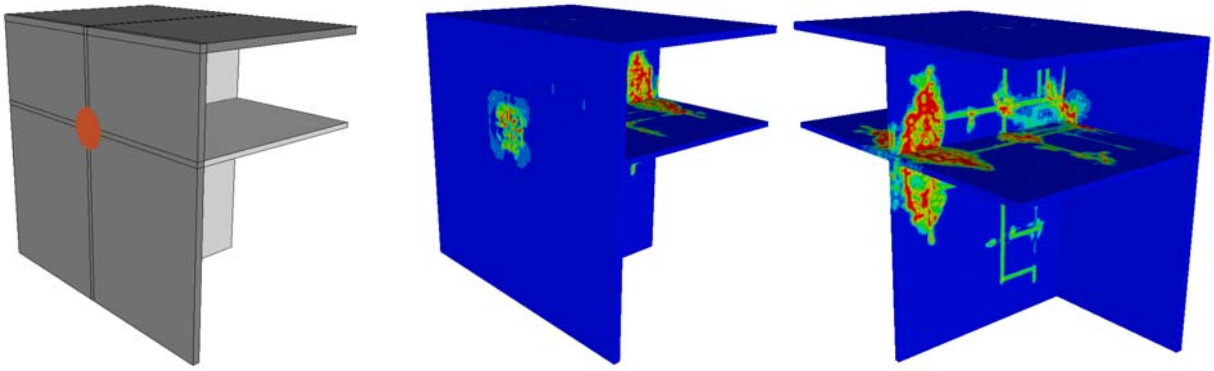

Fig. 7: FE-model (HxWxD = 27x29x20 m³) with airliner impact load on stiffening cross (left); predicted damage on the front face, propagation in depth and wave-induced tensile damage close to the rear wall of the box girder (right)

The calculated damage pattern in Fig. 7 shows that no perforation occurs. A large damage cone develops directly in the bracings behind the front wall. Furthermore, there is an overload in the rear part of the wall resulting from superposition of arriving and reflected stress waves inside the building component. From experiences in similar calculations with mesh-free and mesh-based methods one can infer that the outer extent of the damage cone area is captured realistically despite cracks following orthogonal mesh directions. These results of local loading and damage effects are considered suitable input data for investigations of the global integrity of the building.

CONCLUSIONS

Validated explicit Finite-Element-Methods with separate dynamic constitutive models for concrete and rebar and two-degree-of-freedom models provide especially in combination a reliable basis to predict limit thicknesses of reinforced concrete targets under aircraft impact. A large data base is available for conventional concrete. New experimental studies and numerical models for ultra high performance concrete (f'_c = 160 MPa) allow predictive calculations. Interpolation to high performance concrete qualities (f'_c = 80 MPa) is possible with reasonable confidence, but should be subject to further experimental validation.

With a rebar content of 120 cm²/m and 150 cm²/m stirrups, a monolithic thickness limit of 90 cm to 100 cm is derived for military aircraft and the considered civilian airliner and speed. 110 cm of HPC are necessary considering tensile preloading across the box girder. UHPC offers slight advantages of about 10 cm reduced thickness compared to HPC, not justifying the higher material and design costs in the considered concept study. T-sections of the box-girder structure with thickness of 50 cm show surprisingly low front damage, but extending failure zones along the bracings and a large spall failure zone by tensile wave superposition at the rear wall.

The above analysis provide basic data for the development of the comprehensive structural concept, including the global impact response, induced vibrations and foundation in the part II of the paper.

REFERENCES

[1] Drittler, K., Gruner, P., *Zur Auslegung kerntechnischer Anlagen gegen Einwirkungen von außen, Teilaspekt: Berechnung von Kraft-Zeitverläufen beim Aufprall deformierbarer Flugkörper auf eine starre Wand*, Wissenschaftliche Berichte IRS-W-14, April 1975

[2] Kamil, H., Kost, G., Sharpe, R., Krutzik, W., *Analyses of Critical Structures and Contained Equipment for Aircraft Impact Loading*, 5th Int. Conf. on structural Mechanics in Reactor Technology, Berlin, 1979

[3] *RSK-Leitlinien für Druckwasserreaktoren*, LL DWR, 1979

[4] Jonas, W., Rüdiger, E., Gries, M., Riech, H., Rützel, H., *Kinetische Grenztragfähigkeit von Stahlbetonplatten; Bericht RS 165*, Hochtief AG, Abt. Kerntechnischer Ingenieurbau, Frankfurt, 1982

[5] Riera, J.D., *On the Stress analysis of Structures subjected to Aircraft Impact Forces*, Nuclear Engineering and Design 8, pp. 415–426, 1968

[6] Schlüter, F.-H., *Dicke Stahlbetonplatten unter stoßartiger Belastung - Flugzeugabsturz*, Dissertation, Th Karlsruhe, 1987

[7] *DIN 25449, Bauteile aus Stahl- und Spannbeton in kerntechnischen Anlagen - Sicherheitskonzept, Einwirkung, Bemessung und Konstruktion*, Deutsches Institut für Normung e.V., Beuth, Berlin, 1987

[8] Nöldgen, M., *Modeling of Ultra High Performance Concrete (UHPC) under Impact Loading – Design of a High Rise Building Core against Aircraft Impact*, Forschungsergebnisse aus der Kurzzeitdynamik, Fraunhofer Verlag, Heft 19, 2011

[9] Katayama, M., Itoh, M., Rainsberger, R., *Numerical Simulation of Jumbo Jet Impacting on Thick Concrete Walls*, 2nd Asian Conf. on High Pressure Research (ACHPR-2), Nara, November 2004

[10] Itoh, M., Katayama, M., Rainsberger, R., *Computer simulation of an F-4 Phantom crashing into a reinforced concrete wall*, 2nd Int. Conf. on Computational Ballistics, Cordoba Spain, 18-20 May 2005

[11] Werner Riedel, Nobuaki Kawai and Ken-ichi Kondo, Numerical Assessment for Impact Strength Measurements in Concrete Materials, International Journal of Impact Engineering 36 (2009), pp. 283-293

[12] Nöldgen M., Fehling E., Riedel W., Thoma K., *Impact Safety of structural Ultra High Performance Concrete (UHPC) elements – Combined Numerical and Experimental Approach*, CONSEC 10, June 2010

[13] *Autodyn - Interactive Non-Linear Dynamic Analysis Software*, Theory Manual 4.0, Century Dynamics Inc., Horsham, U.K., 1998.

[14] Johnson, G.R., Cook, W.H., *A Computational Constitutive Model and Data for Metals Subjected to Large Strains, High Strain Rates and High Temperatures*, 7th Int. Symp. Ballistics, Den Haag Niederlande, 1983

[15] Riedel, W., *Beton unter dynamischen Lasten: Meso- und makromechanische Modelle und ihre Parameter*, Fraunhofer - Ernst-Mach-Institut, Freiburg i. Br., 2004, ISBN 3-8167-6340-5

[16] Sugano, T., Tsubota, H., Kasai, Y., Koshika, N., Ohnuma, H., von Risemann,W.A., Bickel, D.C., Parks, M.B., *Local damage to reinforced concrete structures caused by impact of aircraft engine missiles–Part 1. Test program, method and results*, Nuclear Engineering and Design 140, pp. 387–405, 1993

[17] Fehling E., Schmidt M., *Entwicklung, Dauerhaftigkeit und Berechnung Ultra-Hochfester Betone (UHPC)*, Bericht DRG FE 497/1-1, Baustoffe und Massivbau Heft 1, Universität Kassel, ISBN 389958-108-3, 2005

[18] Riedel , Nöldgen , Straßburger , Thoma, Fehling , *Local Damage to Ultra High Performance Concrete Structures caused by an Impact of Aircraft Engine Missiles*, Nucl Engn & Design 240 (2010), 2633

APPENDIX: MATERIAL INPUT DATA

	C 35/45	HPC 80/95	UHPC		C 35/45	HPC 80/95	UHPC
Equation of Sate	p-α			Strength	RHT concrete		
Reference density [g/cm³]	2.750E+00	2.818E+00	2.858E+00	Shear Modulus [kPa]	1.670E+07	2.019E+07	2.080E+07
Porous density [g/cm³]	2.314E+00	2.490E+00	2.510E+00	Compressive Strength (fc) [kPa]	3.500E+04	8.000E+04	1.580E+05
Porous soundspeed [m/s]	2.920E+03	3.571E+03	3.327E+03	Tensile Strength (ft/fc) [-]	1.000E-01	4.900E-02	5.500E-02
Initial compact. pressure [kPa]	2.330E+04	5.333E+04	1.053E+05	Shear Strength (fs/fc) [-]	1.800E-01	1.800E-01	1.000E-01
Solid compact. Pressure [kPa]	6.000E+06	6.000E+06	6.000E+06	Intact Failure Surface Const. A [-]	1.600E+00	2.300E+00	2.010E+00
Compaction exponent [-]	3.000E+00	4.000E+00	4.000E+00	Intact Failure Surface Exp. N [-]	6.100E-01	5.000E-01	6.360E-01
Solid EOS	Polynomial			Tens./Comp. Meridian Ratio Q [-]	6.805E-01	6.805E-01	6.805E-01
Bulk Modulus A1[kPa]	3.527E+07	7.370E+07	8.410E+07	Brittle to Ductile Transition [-]	1.050E-02	1.050E-02	1.050E-02
Parameter A2 [kPa]	3.958E+07	8.070E+07	9.120E+07	G (elas.)/(elas.-plas.) [-]	2.000E+00	1.010E+00	2.310E+00
Parameter A3 [kPa]	9.040E+06	1.450E+07	1.460E+07	Elastic Strength / ft [-]	7.000E-01	8.500E-01	9.500E-01
Parameter B0 = Γ [-]	1.220E+00	8.000E-01	1.160E+00	Elastic Strength / fc [-]	5.300E-01	6.500E-01	7.000E-01
Parameter B1 = Γ [-]	1.220E+00	8.000E-01	1.160E+00	Fract. Strength Constant B [-]	1.600E+00	2.300E+00	2.310E+00
Reference Temperature [K]	3.000E+02	3.000E+02	3.000E+02	Fract. Strength Exponent M [-]	6.100E-01	5.000E-01	6.360E-01
Specific Heat [J/kgK]	6.540E+02	6.540E+02	6.540E+02	Comp. Strain Rate Exp. Alpha [-]	3.200E-02	9.430E-03	6.700E-03
Compaction Curve	Standard			Tensile Strain Rate Exp. Delta [-]	3.600E-02	1.290E-02	7.800E-03
Erosion	Geometric Strain			Failure	RHT Concrete		
Erosion Strain [-]	5.000E-01	5.000E-01	5.000E-01	Damage Constant, D1[-]	4.000E-02	4.000E-02	4.000E-02
Tens./Comp. Meridian Ratio $Q_{2.0}$ [-]	6.805E-01	6.805E-01	6.805E-01	Damage Constant, D2 [-]	1.000E+00	1.000E+00	1.000E+00
Brittle to Ductile Transition B [-]	1.050E-02	1.050E-02	1.050E-02	Minimum Strain to Failure [-]	1.000E-02	1.000E-02	1.000E-02
				Tensile Failure	Hydro (Pmin)	Principal Stress	
Fracture Energy, Gf [J/m²]	-	5.000E+03	1.000E+04	Princ. Tensile Failure Stress [kPa]	-	7.500E+03	4.200E+04

BSt500 reinforcement			
Equation of State	Linear	Strength	Johnson Cook
Reference density [g/cm³]	7.830E+00	Shear Modulus [kPa]	8.180E+07
Bulk Modulus [kPa]	1.590E+08	Yield Stress [kPa]	4.500E+05
Reference Temperature [K]	3.000E+02	Hardening Constant [kPa]	5.100E+05
Specific Heat [J/kgK]	4.770E+02	Hardening Exponent [-]	2.600E-01
Failure	Plastic Strain	Strain Rate Constant [-]	1.400E-02
Plastic Strain [-]	1.600E-01	Thermal Softening Exponent [-]	1.030E+00
Erosion	Geometric Strain	Melting Temperature [K]	1.793E+03
Geometric Strain [-]	1.666E-01	Ref. Strain Rate [1/s]	1.000E+00